Aqueous Transition Metal Cations as Impurities in a Wide Gap Oxide: The Cu^{2+}/Cu^{1+} and Ag^{2+}/Ag^{1+} Redox Couples Revisited

Xiandong Liu,[*,†,‡] Jun Cheng,[†,¶] and Michiel Sprik[†]

Department of Chemistry, University of Cambridge, Cambridge CB2 1EW, United Kingdom, State Key Laboratory for Mineral Deposits Research, School of Earth Sciences and Engineering, Nanjing University, Nanjing 210093, P. R. China, and Department of Chemistry, University of Aberdeen, Aberdeen AB24 3UE, United Kingdom

E-mail: xiandongliu@nju.edu.cn

[*]To whom correspondence should be addressed
[†]University of Cambridge
[‡]Nanjing University
[¶]University of Aberdeen

Abstract

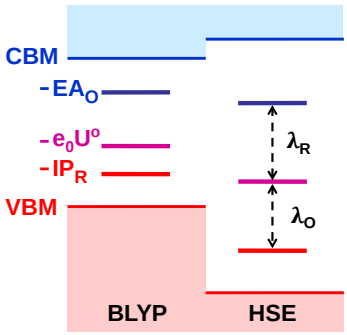

The interactions of the *d* electrons of transition metal aqua ions with the solvent are usually divided in short range electronic interactions with ligand water molecules and long range electrostatic interactions with molecules beyond the first coordination shell. This is the rationale behind the cluster continuum and QM/MM methods developed for the computation of the redox potentials. In the density functional theory based molecular dynamics (DFTMD) method the electronic states of the complex are also allowed to mix with the extended band states of the solvent. Returning to the Cu^{1+} and Ag^{1+} oxidation reaction which has been the subject of DFTMD simulation before we show that coupling to the valence band states of water is greatly enhanced by the band gap error in the density functional approximation commonly used in DFTMD (the generalized gradient approximation). This effect is analyzed by viewing the solvent as a wide gap oxide and the redox active ions as electronic defects. The errors can be reduced significantly by application of hybrid functionals containing a fraction of Hartree-Fock exchange. These calculations make use of recent progress in DFTMD technology enabling us to include *sp* core polarization and Hartree-Fock exchange in condensed phase model systems.

Keywords

Aqueous redox chemistry, computational chemistry, density functional theory

Introduction

Ionization energies of atoms strongly depend on the oxidation state. The more electrons have been taken away the higher is the energy for removing the next electron. Solvation drastically reduces this progressive increase in ionization energy and transition metal aqua cations generally have more than one accessible oxidation state. The free energy for a change of oxidation state is given by the standard reduction potential U°. Measured relative to vacuum U° values are in the range of 3 to 6 Volt. For cations, redox potentials differ from the corresponding vacuum ionization potentials by one order of magnitude or more. Accurate reproduction of experimental redox potentials is therefore a bench mark test for the methods of condensed phase computational chemistry. To be useful for applications, e.g. in catalysis, errors should not exceed 200 mV (3 pK units at ambient temperature).

Metal aqua ions are among the more challenging systems for computational electrochemistry.[1] Modern implicit solvent methods have, on the whole, been successful in meeting the 200 mV accuracy requirement[2–7] although there remain some difficult cases (for a critical assessment and a comprehensive list of references see Ref. 1). These methods treat the metal ion and a small number of coordinated water molecules at the level of an accurate electronic structure calculation method while the bulk solvent is represented by a continuum reaction field (implicit solvent model). Experience has shown that the full first coordination shell as well as the second coordination shell of H_2O should be included in the quantum calculation.[2–5] In this form the implicit solvent scheme is often referred to as the cluster-continuum method. The increased system size makes in practice Density Functional Theory (DFT) the method of choice. On the next level of atomic detail the implicit solvent is replaced by an explicit water model derived from a classical force field. This approach is generally known as the QM/MM method. Both non-polarizable[8] and polarizable water force fields have been considered.[1]

In a truly uncompromising first principle approach all of the solvent is treated at the same DFT level as the metal ion(all-atom method).[9–14] Aqueous solvents are liquids and all-atom

methods must be combined with molecular dynamics (MD) sampling. This approach will be referred to as density functional theory based molecular dynamics (DFTMD).[15,16] Finite temperature fluctuations of coordination geometry and hydrogen bonding are now explicitly accounted for as is the effect of interaction with the extended (band) states of the solvent. DFTMD comes of course at the expense of a huge increase in computational costs.

Unfortunately, the increase in computational effort also tends to increase the errors in U°. The same DFT approximations (the generalized gradient approximation and hybrid functionals) do better when implemented with the cluster-continuum or QM/MM approach. This seems to be the at first somewhat counter intuitive conclusion of our DFTMD calculation of the oxidation potential of a set of small aqua anions ($Cl^-, OH^-, SH^-, HO_2^-, O_2^-, CO_2^-$).[17] The experimental reduction potentials of this series, ordered here according to decreasing oxidation power, vary from +2.41 V for Cl/Cl^- to −1.8 V for CO_2/CO_2^-.[18] These aqueous species are still small enough to be amenable to DFTMD treatment. Inaccuracies due to finite system size and duration of the MD sampling can be kept below 0.2V. The DFT related error is significantly larger. In particular, the BLYP functional,[19,20] favoured in DFTMD studies of aqueous systems, systematically underestimates the redox potential. The error is linear in U° varying from almost 1.0 V at the positive end of the series (Cl/Cl^-) to essentially 0.0 V at the negative end (CO_2/CO_2^-).

The explanation for the systematic underestimation of U° in the generalized gradient approximation (GGA) becomes clear when the vertical ionization potential (IP) of the reduced state (the anion) is compared to experiment. Vertical IP's are a more direct probe of electronic structure. Thanks to progress in liquid microjet photo emission spectroscopy (PES)[21,22] this critical test of the performance of electronic structure calculation methods has become possible also for valence electrons in molecular liquids. In particular the Winter group in Berlin has determined the vertical IP of a series of model aqueous species, such as inorganic anions, including the hydroxide,[23] halide[23] and phosphates anions,[24] small organic anions,[25,26] and recently also of neutral molecules[27] and transition metal cations.[5,13,14] As

an instructive example of how these measurements of vertical IP's can be used to validate computational methods we mention a recent study on how many explicit water molecules must be included in the continuum cluster calculation of the ionization energy of aqueous phosphate anions in various protonation states.[24]

The aqueous hydroxide anion

Among aqueous ions, the hydroxide anion plays a special role because it is an ionization product of the solvent itself. This is why we have chosen the solvated OH^- as the key test system in the development of our all-atom computational methods.[17,28–30] Starting with the pioneering work by Delahay,[31,32] the aqueous OH^- has also been a popular model system for application of electronic spectroscopy to aqueous solution.[23,33] The PES measurements of Ref. 23 give 9.2 eV for the vertical IP of OH^-(aq). To compare to the reduction potential of the $OH^\bullet/OH^-$ couple we convert the absolute IP to the Standard Hydrogen Electrode (SHE) scale by subtracting the absolute SHE potential.[34,35] This gives $9.2 - 4.44 = 4.8$ V which is significantly higher than the 1.90 V *vs* SHE for the reduction potential.[18] The 2.9 V difference can be interpreted as reorganization energy of the aqueous environment.[28,31,32] The corresponding BLYP/DFTMD estimates we computed in Ref. 17 are 2.1 V for the IP and 1.3 V for U° again using the SHE as common energy reference.

What this quick comparison first of all shows is that the DFT error is strongly enhanced in the vertical IP. The discrepancy between experimental and calculated vertical IP's (2.7V) is more than four times larger than the discrepancy between the reduction potentials (0.6 V). In Ref. 17 we attributed this effect to mixing with the valence band of water. Identifying the photo emission threshold with the valence band maximum (VBM), the measurements of the Berlin group place the VBM at 9.9 eV relative to vacuum[23,36] corresponding to 5.5V *vs* SHE. Using BLYP we found a significantly smaller value,[37,38] namely 2.3V on the SHE scale. Consistent with the IP of OH^-(aq) the vertical IP of liquid water is badly underestimated at the GGA level. The ionizable occupied one-electron energy levels end up well above where

they should be. Moreover the gap between the IP of OH^- and the VBM of water, which was $5.5-4.8=0.7$eV in experiment has been reduced by BLYP to as little as $2.3-2.1=0.2$ eV. A similar effect has been observed for the chloride anion.[39,40] The near degeneracy makes it easy for the localized highest occupied molecular orbital (HOMO) of the solute to mix with the extended states of the solvent (a more accurate picture is that the small gap is the result of a resonance between the localized solute level and the valence band of the solvent[17]).

The vanishing gap between HOMO of the solvated OH^- and the VBM of water could be dismissed as a DFT artefact. However, also in experiment the electron detachment level of OH^- is sufficiently close to the VBM of water that some degree of hybridization cannot be excluded. Following a parallel to charged defects in semiconductors[41–49] we suggested therefore in Ref. 17 that aqueous hydroxide can be viewed as a shallow defect (an hydrogen vacancy) in a wide gap oxide (water). The implication is that hybridization with the valence band of water itself cannot be the main cause of the underestimation of the IP of OH^-. Rather, it is the misalignment of the VBM that pushes up the HOMO of OH^- and of any other solute with a vertical IP close to the VBM of water, such as the Cl^- ion.[23,39,40] In fact the underestimation of the IP of these anions is another case of the band gap error in DFT identified by computational solid state physicists as the explanation of the error in charge state transition levels of defects.[41–44,46,47] The electron attachment levels (minus the vertical electron affinity (EA) of the oxidized state) are further removed from the misaligned VBM. The vertical EA is less affected and therefore also the reduction potentials which depend on both the IP of the reduced and the EA of the oxidized state.[17,38] It also explains the observation we made in Ref. 17 that the errors in the reduction potentials less oxidative species are less serious.

The error analysis above could not have been carried out without a molecular dynamics hydrogen electrode (MDHE) enabling us to compare redox potentials of half reactions and the corresponding vertical ionization potentials to experiment. Our implementation of a MDHE was developed in two key technical papers.[50,51] Electronic energies are directly

referred to the solvation free energy of H^+ computed from reversible insertion of a proton. This technique, combining DFTMD and free energy perturbation, was originally developed for the computation of acidity constants (pKa).[52] No such computational tool was available in our earlier studies of redox properties of transition metal aqua ions.[9–11] All we could do was comparing the free energies of a pair of redox half reactions, one reactant oxidizing the other. As already indicated, the leading inaccuracy in DFTMD half reaction free energies is related to removal/addition of electrons from/to condensed phase systems. These errors are concealed (cancelled) to some extent in full electron transfer reactions. The hydrogen electrode, however, removes a proton from the solution with the electron is added in vacuum. Coupling of such a closed shell reaction to a redox half reaction lifts the cancellation of errors in electron transfer reactions fully exposing these errors to scrutiny.

A further limitation of our earlier work is the density functional approximation which was restricted to the generalized gradient approximation (GGA). Application of hybrid functionals containing a fraction of exact exchange was not feasible. The increase in computational costs due to the periodic boundary conditions in DFTMD was too high. Thanks to recent technical advances the overhead of exact exchange in extended systems has been significantly reduced.[53] DFTMD simulation using hybrid functionals has become (almost) routine. Finally, there is a third more technical feature of the current state of the art of DFTMD reduction potential calculation not available in earlier work. These simulations were carried out using the CPMD code.[54] The molecular orbitals of valence electrons in CPMD are expanded in a plane wave basis set in combination with soft pseudo potentials of the Troullier-Martins type[55] representing core electrons. In our more recent work we switched to the CP2K code,[56] which uses a localized Gaussian basis set and harder pseudopotentials of the Goedecker-Teter-Hutter type.[57,58] In practice this means that CP2K allows us to extend the valence electrons of an ion with redox active *d* electrons to the full *spd* shell. This was not feasible in CPMD. This may be relevant in particular for the study of redox properties of 3d transition metal ions.

The Cu and Ag aqua cations

These three innovations, molecular dynamics hydrogen electrode, hybrid functionals and polarizable core electrons, all implemented in the CP2K code,[56] motivated us to return to the redox reactions we studied in our very first attempt at computing DFTMD reduction potentials,[9] namely the Cu^{2+}/Cu^{1+} and Ag^{2+}/Ag^{1+} reductions. In hindsight the one-electron oxidation of the Cu^{1+} and Ag^{1+} aqua ions should be an almost ideal example to illustrate the effect of the proximity the VBM of water. Similar to the OH^- and Cl^- anions, these group IB cations are closed shell. The experimental value of U° for Ag^{2+}/Ag^{1+} is 1.98 V *vs* SHE.[59] The Ag^{2+} is therefore a most aggressive oxidant with an oxidizing power similar to $OH^\bullet$ and should therefore be equally prone to interaction with the extended state of water. The redox potential for Cu^{2+}/Cu^{1+}, rather surprisingly, is only 0.16 V *vs* SHE.[59] The Cu^{2+} is redox neutral, and should, according to our theory, be less sensitive to the band gap error in DFT. The calculations we will compare to are from Ref. 11 for Ag^{2+}/Ag^{1+} and from Ref. 12 for Cu^{2+}/Cu^{1+}. The very first calculations in Ref. 9 were based on a completely different scheme[60,61] which we no longer use.

Anticipating our results, we find that the Cu^{2+}/Cu^{1+} and Ag^{2+}/Ag^{1+} reduction potentials agree with experiment within the 200-300 mV accuracy we set as our target, provided the full machinery described above is applied plus a further finite size correction. We have also applied the MDHE scheme to the calculations of Refs. 11 and 12. Converted to the SHE scale the half reaction free energies can again be separately compared to experiment. The U° for Cu^{2+}/Cu^{1+} is 1.3 V lower than the best value computed here. The U° for Ag^{2+}/Ag^{1+} is 1.6 V lower. As expected, the decrease in the strongly positive potential of the Ag^{2+}/Ag^{1+} couple is dominated by the change over from a GGA(BLYP[19,20]) to a hybrid functional(HSE06[62]). The potential of the redox neutral Cu^{2+}/Cu^{1+} couple is less sensitive to the introduction of exact exchange. The other way around, freezing the core electrons has more of an effect on Cu^{2+}/Cu^{1+}(3d) than on Ag^{2+}/Ag^{1+}(4d).

Also the solvent relaxation is note quite the same. In the old scheme the response to a

change of charge of the ions appeared to be distinctly non-linear.[11,12] Treated at the highest level of approximation in the new scheme, the non-linearity is less pronounced. Blumberger argued in Ref. 12 that non-linear solvent response is to be expected for Cu^{2+}/Cu^{1+} because of the rather drastic change of the number of water molecules in the first solvation shell. The accuracy of our calculations still allows for such a non-linear effect. The reorganization of the solvent in the Ag^{2+}/Ag^{1+} reaction, on the other hand, is now effectively in accordance with the linear response approximation of Marcus theory. The observations for Ag^{2+}/Ag^{1+} are therefore consistent with our results for the hydroxide ion[17] (recall the redox potentials are virtually the same). Similar to the $OH^{\bullet}/OH^{-}$ couple, symmetry is essentially restored when calculated using HSE06.

It should be clear by now that the presentation in this paper is rather technical focusing on issues that were confusing to (at least) the authors. We start therefore with a brief summary of the theory and method in its current formulation. Next, the results are presented and analyzed. In the summary and outlook we return to the parallel with charged defects in wide gap oxides and address the question under what conditions all-atom DFTMD methods could be of use (or rather worth the effort) in the computational study of aqueous redox chemistry.

Theory and method

Workfunctions and half reactions

The formal basis of our method is Trasatti's theory of absolute electrode potentials.[34] We follow the presentation of Ref. 38 reformulated for the one-electron reduction of an aqua cation M^{q+1} of charge $q+1$

$$M^{q+1} + e^{-} \rightarrow M^{q} \tag{1}$$

The standard reduction potential *vs* SHE of this homogeneous half reaction is defined by the standard free energy change of the reaction

$$\mathrm{M}^{q+1} + \frac{1}{2}\mathrm{H}_2(\mathrm{g}) \rightarrow \mathrm{M}^{q} + \mathrm{H}^{+}(\mathrm{aq}) \tag{2}$$

and can be expressed as the sum of an electronic and ionic work function

$$e_0\, U_q^{\circ}(\mathrm{she}) = \mathrm{AIP}_q(\mathrm{abs}) + \mathrm{W}_{\mathrm{H}^+}(\mathrm{abs}) - \mu_{\mathrm{H}^+}^{g,\circ} \tag{3}$$

$\mathrm{AIP}_q(\mathrm{abs})$ is the *adiabatic* ionization potential of M^q in aqueous solution and $\mathrm{W}_{\mathrm{H}^+}(\mathrm{abs})$ the workfunction of the aqueous proton ($\mathrm{H}^+(\mathrm{aq})$). The (abs) extension has been added as a reminder that these quantities are absolute workfunctions referred to a point in vacuum just outside the surface of the electrolyte.[34,35] Note that we have have simplified the notation for the reduction potential of the $\mathrm{M}^{q+1}/\mathrm{M}^q$ couple suppressing the specification of the metal species M. $\mu_{\mathrm{H}^+}^{g,\circ}$ is the standard chemical potential of the gas-phase proton ($\mathrm{H}^+(\mathrm{g})$) obtained form the free energy of the reaction $\frac{1}{2}\mathrm{H}_2(\mathrm{g}) \rightarrow \mathrm{H}^+(\mathrm{g}) + e^-(\mathrm{vac})$. e_0 is the elementary charge (microscopic energy units are used). The last two terms of Eq. 3 add up to the negative of the absolute SHE potential:[34]

$$U_{\mathrm{H}^+/\mathrm{H}_2}^{\circ}(\mathrm{abs}) = \frac{1}{e_0}\left(\mu_{\mathrm{H}^+}^{g,\circ} - \mathrm{W}_{\mathrm{H}^+}\right) \tag{4}$$

The value of $U_{\mathrm{H}^+/\mathrm{H}_2}^{\circ}(\mathrm{abs})$ recommended in Ref. 34 is 4.44 V. This estimate was the result of a critical comparison of experimental data from various sources available at the time and has now been accepted as accurate within a 10 or 20 mV margin.[35]

The adiabatic IP in Eq. 3 is a *free* energy difference between oxidation states which is not directly accessible in electronic structure calculation. However free energy differences can be related to total energy differences using coupling integral methods.[63] A fictitious mapping Hamiltonian $\mathcal{H}_\eta$ is constructed consisting of a linear combination $\mathcal{H}_\eta = \eta\mathcal{H}_\mathrm{O} + (1-\eta)\,\mathcal{H}_\mathrm{R}$ of

the atomic Hamiltonian $\mathcal{H}_{\mathrm{O}}$ of the oxidized state (M^{q+1}) and $\mathcal{H}_{\mathrm{R}}$ of the reduced state (M^{q}). The coupling parameter connecting R and O takes the values $0 \leq \eta \leq 1$. The thermodynamic integration is carried out under full 3D periodic boundary conditions (pbc). The result is the free energy for the reversible removal of an electron from the periodic model system

$$\mathrm{AIP}_q(\mathrm{pbc}) = \int_0^1 d\eta \, \langle \Delta E_q(\mathrm{pbc}) \rangle_\eta \tag{5}$$

Where $\Delta E_q(\mathrm{pbc})$ is the vertical IP of M^q computed from total energy differences. The brackets denote a thermal average over the canonical ensemble defined by $\mathcal{H}_\eta$.

Full 3D periodic boundary conditions leave no interfaces to vacuum. Without such an interface the reference of the electrostatic potential is ill-defined leading to the infamous band alignment problem of computational solid state physics. The uncertainty in the zero of the electrostatic potential has no effect on total energies of neutral systems but shows up in ionization (single particle) energies. The electronic work function $\mathrm{AIP}_q(\mathrm{pbc})$ of Eq. 5 can therefore not be identified with the absolute work function $\mathrm{AIP}_q(\mathrm{abs})$ of Eq. 3 but differs from it by a constant playing the role an effective bias V_0 in the electrostatic reference

$$\mathrm{AIP}_q(\mathrm{abs}) = \mathrm{AIP}_q(\mathrm{pbc}) + e_0 V_0 \tag{6}$$

For electronic structure calculation methods as applied here, V_0 in Eq. 6 is positive and typically in the order of several eV. It depends on composition but is also sensitive to details of the electronic structure calculation, including non-physical constructs such as pseudo potentials.

The net cell reaction in an electrochemical device conserves charge and so does reaction Eq. 2 defining the SHE potential of reaction Eq 1. Potentials referred to the SHE should therefore be invariant under shifts in the zero of the electrostatic potential. Indeed, the absolute workfunction $W_{\mathrm{H}^+}(\mathrm{abs})$ in Eq. 3 and the reversible work $W_{\mathrm{H}^+}(\mathrm{pbc})$ for removing a proton from the periodic model system differ by an offset opposite to the one for electrons

(Eq. 6) because the proton has a positive elementary charge

$$W_{\mathrm{H^+}}(\mathrm{abs}) = W_{\mathrm{H^+}}(\mathrm{pbc}) - e_0 V_0 \tag{7}$$

$W_{\mathrm{H^+}}(\mathrm{pbc})$ is again estimated from a thermodynamic integral similar to Eq. 6

$$W_{\mathrm{H^+}}(\mathrm{pbc}) = \int_0^1 d\eta \, \langle \Delta E_{\mathrm{H_3O^+}}(\mathrm{pbc}) \rangle_\eta - \Delta E_{\mathrm{zp}} \tag{8}$$

$\Delta E_{\mathrm{H_3O^+}}$ is the energy for vertical deprotonation of a hydronium ion (H_3O^+). ΔE_{zp} is a zero point motion correction. The modelling of desolvation of H^+ by deprotonation of H_3O^+ is an approximation originally introduced for the calculation of acidity constants.[52] The implementation and justification of this scheme is outlined in detail in Refs. 50 and 51.

Substituting Eqs. 5 and 8 in Eq. 3 we find

$$U_q^\circ(\mathrm{she}) = \frac{1}{e_0} \mathrm{AIP}_q(\mathrm{pbc}) - U^\circ_{\mathrm{H^+/H_2}}(\mathrm{pbc}) \tag{9}$$

where $U^\circ_{\mathrm{H^+/H_2}}(\mathrm{pbc})$ is the MDHE potential

$$U^\circ_{\mathrm{H^+/H_2}}(\mathrm{pbc}) = \frac{1}{e_0} \left(\mu^{g,\circ}_{\mathrm{H^+}} - \mathrm{W}_{\mathrm{H^+}}(\mathrm{pbc}) \right) \tag{10}$$

Eq. 9 suggests that the ionization of the solute and insertion/removal of a proton can be carried out independently in separate periodic model systems. The advantage of such a half reaction scheme is that the (expensive) computation of the proton work function needs to be carried only once for a given system geometry. This is how the homogeneous redox potentials and acidities have been computed in our previous publications since the introduction of the MDHE.[17,28,37,50–52] The condition for the validity of the half reaction scheme is, of course, that V_0 is the same in both half cells.

A further advantage of the half reaction scheme is that it can be equally employed to

obtain estimates of vertical ionization potentials IP_q of M^q and the vertical electron affinities EA_{q+1} of M^{q+1} directly referred to the SHE. These two states are connected by the coupling parameter integral Eq. 5 and we can write

$$\mathrm{IP}_q(\mathrm{she}) = \langle \Delta E_q(\mathrm{pbc}) \rangle_{\eta=0} - e_0 U^{\circ}_{\mathrm{H^+/H_2}}(\mathrm{pbc}) \tag{11}$$

and similarly

$$\mathrm{EA}_{q+1}(\mathrm{she}) = \langle \Delta E_q(\mathrm{pbc}) \rangle_{\eta=1} - e_0 U^{\circ}_{\mathrm{H^+/H_2}}(\mathrm{pbc}) \tag{12}$$

The value given in Ref. 51 for the standard MDHE potential $U^{\circ}_{\mathrm{H^+/H_2}}(\mathrm{pbc}) = 0.81\mathrm{V}$. This estimate was obtained by protonating a water molecule in the "standard" DFTMD water model of 32 H_2O molecules in a cubic MD cell of length 9.86 Å. The functional used in Ref. 51 is BLYP. We repeated the calculation using HSE06 in exactly the same system geometry applying the same corrections for zero point motion[51] and found $U^{\circ}_{\mathrm{H^+/H_2}}(\mathrm{pbc}) = 0.75\mathrm{V}$. The difference between the BLYP and HSE06 estimate is well below the error margin (0.2 eV) and we therefore decided to convert all our ionization potentials to the SHE scale using $U^{\circ}_{\mathrm{H^+/H_2}}(\mathrm{pbc}) = 0.81\mathrm{V}$ independent of the functional.

The 3.63 V difference between $U^{\circ}_{\mathrm{H^+/H_2}}(\mathrm{pbc})$ and the experimental absolute SHE potential $U^{\circ}_{\mathrm{H^+/H_2}}(\mathrm{abs}) = 4.44\mathrm{V}$ can be interpreted as an estimate of V_0 in Eqs. 6 and 7. V_0 has been calculated by other authors using pseudo potential/plane wave methods.[64–67] While differing in the detailed implementation, these four calculations should give comparable results. The average is $V_0 = 3.6\mathrm{V}$ with a variance of 0.3 V. However, it should be kept in mind that V_0 depends on the shape of the PP in the core region. Details in pseudization procedure can easily give rise to discrepancies in the order of 0.3 V. In particular, even though the valence of the PP is the same, the q11 PP used in CPMD calculations (Trouillier-Martins[55]) is significantly softer compared to the dual space PP's[57,58] used in CP2K. Differences of a few 100 mV between V_0 and by implication $U^{\circ}_{\mathrm{H^+/H_2}}(\mathrm{pbc})$ cannot be excluded. Indeed, the estimate obtained for V_0 in the CPMD calculation of Ref. 64 is 4.0 V compared to the 3.6 V

for CP2K. We note however that V_0 in Ref. 64 was obtained by extrapolation of the ionization energy of vacuum cluster (maximum cluster size is 10 H_2O molecules) to bulk solution and is subject to large uncertainties (1 V or more). A fully consistent comparison between the CPMD and CP2K q11 results, therefore, requires, in principle, repeating the computation of the free energy for reversible insertion of a proton.[51] This expensive calculation has not been carried out. Failing a reliable estimate of $U^{\circ}_{H^+/H_2}$(pbc) for CPMD, we have used he same value (0.81 V) as for CP2K, even though, as explained above, $U^{\circ}_{H^+/H_2}$(pbc) is not strictly transferable. The corresponding uncertainty in the energy reference is smaller than the discrepancies due to the approximations in the DFT (functional and PP).

As a conclusion of this method section we want to reiterate that the numerical value of V_0 is implicit in our approach. Adiabatic (Eq. 9) as well as vertical one-electron energies (Eqs. 11 and 12) are computed directly as potentials *vs* SHE. Explicit specification of V_0 is not necessary. In particular, the question whether or not to correct for the water surface potential[68] is not relevant for us. Comparison to photo emission spectroscopy experiments are made by subtracting 4.44 V from the *experimental* ionization energies which in fact includes a contribution of the water surface potential.[35,38]

Electronic structure calculation

All simulations were carried out using the CP2K/QUICKSTEP package.[56,69] The molecular orbitals are expanded in a hybrid Gaussian plane wave (GPW) basis set[70] using Goedecker-Teter-Hutter pseudopotentials to represent core electrons.[57,58] The valence configurations of H and O are $1s^1$ and $2s^2 2p^4$. For the Cu and Ag cations we applied two alternative sets of pseudo potentials based on 11 and 19 valence electron configurations, i.e., $3d^{10}4s^1$ and $3s^2 3p^6 3d^{10} 4s^1$ for Cu and $4d^{10}5s^1$ and $4s^2 4p^6 4d^{10} 5s^1$ for Ag. The plane wave kinetic energy cut off is set to be 280 Ry. The BLYP[19,20] and HSE06[62] functionals are used to model the exchange-correlation. Exact exchange under periodic boundary conditions was implemented using the auxiliary density matrix method of Ref. 53.

Model system and MD

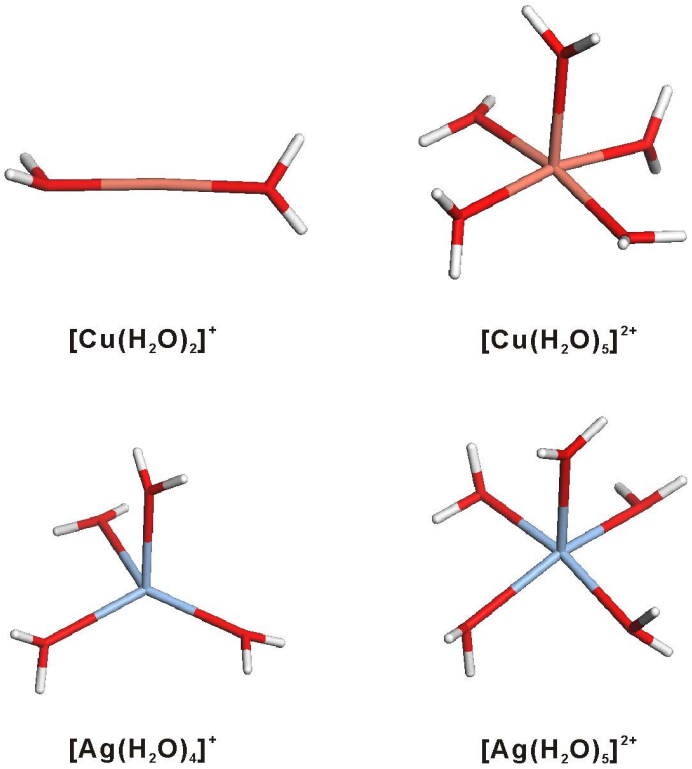

Figure 1: Structures of the $[Cu(H_2O)_2]^+$, $[Cu(H_2O)_5]^{2+}$, $[Ag(H_2O)_4]^+$ and $[Ag(H_2O)_5]^{2+}$ complexes investigated in the gas-phase calculation.

Gas phase calculations are carried out in a cubic box of 20Å. The Martyna-Tuckerman scheme is employed as the Poisson solver in order to eliminate interactions with periodic images[71] For Cu^{1+} and Cu^{2+} we selected the two and five coordinated complexes $[Cu(H_2O)_2]^+$ and $[Cu(H_2O)_5]^{2+}$, for Ag^{1+} and Ag^{2+} the four and five coordinated complexes $[Ag(H_2O)_4]^+$ and $[Ag(H_2O)_5]^{2+}$ (see fig. 1). The geometry is optimized using the BFGS (Broyden-Fletcher-Goldfarb-Shannon) method. Five coordinated complex can have more than one stable geometry as suggested by the MD trajectories in solution which show transformation between pyramidal and trigonal bi-pyramidal structures. For the gas-phase cluster we only investigated the pyramidal structure.

The solution MD cell is a cubic box of length 9.86Å. The system consists of one metal cation surrounded by 32 water molecules, which approximately represents the density of liq-

uid water at ambient conditions. The MD propagation uses the Born-Oppenheimer method with a wave function optimization tolerance of 1.0E-06. The time step is 0.5 fs. The temperature is controlled by a Nosé-Hoover chain thermostat targeted at 330 K. The elevated temperature is to avoid the glassy behaviour of DFT liquid water. For all values of the coupling parameter (η) the system was initiated from a configuration for the stable d^{10} monocation. Each system is equilibrated for at least 2.0 ps followed by a production run of 5.0 ps to 10.0 ps. The relatively short duration of DFTMD runs is always reason for some concern. The primary result of the DFTMD calculation are vertical energy gaps at selected values of the coupling parameter η from which the redox free energies are obtained by a numerical quadrature estimate of the thermodynamic integral Eq. 5. Figure 2 shows representative examples of the average of the vertical energy gap accumulating over run time. Consistent with previous experience averages of a vertical energy gap seem to converge on a pico second time scale. Averaging over 5 to 10 ps is sufficient to bring the statistical down below 100 meV. A possible explanation for this rather rapid convergence is suggested by the Debye theory of dielectric relaxation. According to this theory the relaxation in response to a sudden change in the charge of a solute proceeds on the time scale of the longitudinal dielectric relaxation time $\tau_L = \tau_D/\epsilon_0$. The Debye relaxation time is indeed in the order of 10ps. The longitudinal relaxation is more than a magnitude faster.

Results and analysis

Gas-phase

Table 1 lists the calculated M-O bond lengths in the four gas-phase complexes we have investigated (see fig. 1). One can see that for the same number of valence electrons, HSE06 predicts a more compact hydration shell compared to BLYP. $[Cu(H_2O)_2]^+$ is a linear complex. The two BLYP calculations give Cu-O bond lengths of 1.90Å. The HSE results are 0.01-0.02Å shorter. $[Ag(H_2O)_4]^+$ is a distorted tetrahedron. The bond lengths according to q19-HSE06

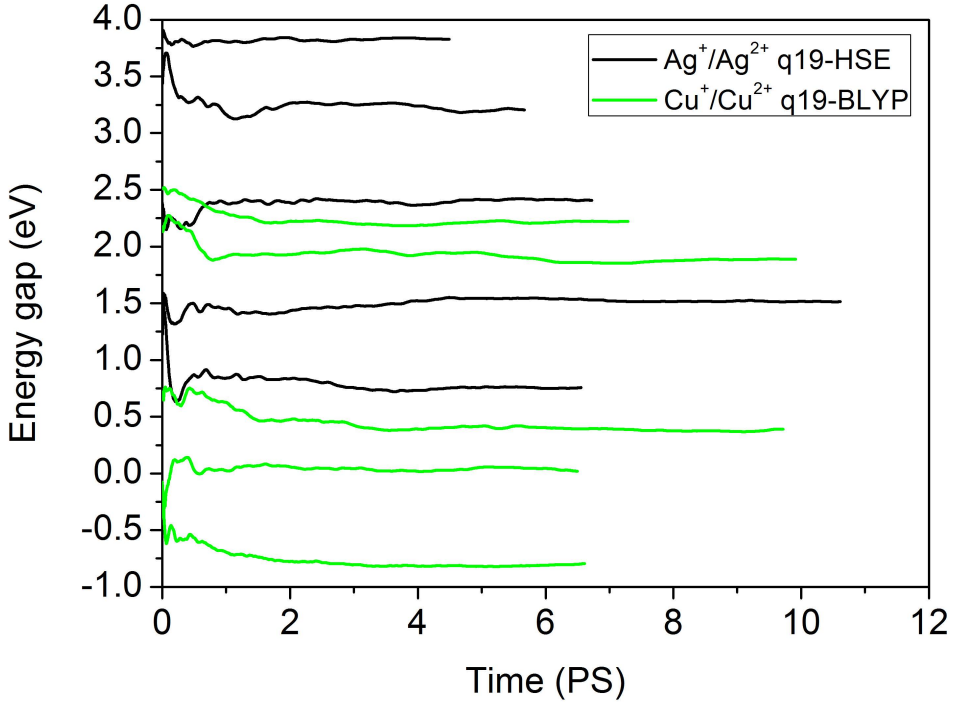

Figure 2: Convergence with time of the average of the vertical ionization energy. Shown are the accumulating average along a typical DFTMD trajectory of the Cu^{2+}/Cu^{1+} and Ag^{2+}/Ag^{1+} system for five values of the couple parameter, $\eta = 0, 0, 25, 0.5, 0.75, 1$.

Table 1: Metal oxygen bond lengths (in Å) in the geometry optimized gas-phase complexes (see fig. 1.

	q11		q19	
	BLYP	HSE	BLYP	HSE
$Cu^{1+}(H_2O)_2$	1.90	1.88	1.90	1.89
$Cu^{2+}(H_2O)_5$	2.18	2.07	2.24	2.16
	2.06/2.06/2.01/2.01	2.06/2.06/1.99/1.99	2.05/2.05/2.02/2.01	2.01/2.00/1.97/1.97
$Ag^{1+}(H_2O)_4$	2.18	2.07	2.24	2.16
$Ag^{2+}(H_2O)_5$	2.43	2.40	2.54	2.50
	2.42/2.37/2.32/2.25	2.24/2.22/2.19/2.16	2.38/2.35/2.30/2.27	2.23/2.22/2.19/2.17

are 0.02-0.05Å shorter than computed with q19-BLYP. For the longest Ag-O bond, q11-HSE06 finds 2.40Å, which is 0.14Å smaller than the maximum bond length in the q11-BLYP geometry. In $[Cu(H_2O)_5]^{2+}$, application of HSE06 reduces the axial Cu-O bonds compared to BLYP. The equatorial bond lengths are similar. For the $[Ag(H_2O)_5]^{2+}$ complex all HSE06

Table 2: Vertical energy gaps (in eV) for the gas-phase complexes of table 1. The numbers in parentheses following the q19-BLYP and q19-HSE06 results denote the increase relative to the corresponding q11 values.

	q11		q19	
	BLYP	HSE	BLYP	HSE
$Cu^{1+}(H_2O)_2$	15.22	14.75	15.52 (0.30)	15.37 (0.62)
$Cu^{2+}(H_2O)_5$	10.42	9.59	10.74 (0.32)	10.48 (0.89)
$Ag^{1+}(H_2O)_4$	13.51	13.96	13.63 (0.12)	14.72 (0.76)
$Ag^{2+}(H_2O)_5$	12.06	11.55	12.25 (0.19)	12.44 (0.89)

Ag-O bonds are shorter. The contraction induced by HSE06 is more obvious for equatorial than for axial bonds. The effect of core state relaxation on the geometry of $[Cu(H_2O)_2]^+$ is not significant. It is more pronounced for the other three complexes, e.g. the difference in the axial Ag-O bond in $[Ag(H_2O)_5]^{2+}$ between q11-BLYP and q19-BLYP is as large as 0.11Å.

The corresponding vertical energy gaps are given in table 2. It is evident that inclusion of core states increases the vertical energy gaps. While this applies to the GGA as well as the hybrid functional calculation, the effect for HSE06 is considerably bigger than for BLYP.

Radial distribution functions

To characterize the hydration in solution we have computed, as usual, the RDF (radial distribution function) and CN (coordination number) of the water O atoms averaging over a MD trajectory with the central metal ion as reference (fig. 3). The CNs confirm the sensitivity of the coordination of the Cu aqua cation to the oxidation state as observed in earlier publications.[9,12] The 5-coordinated $[Cu(H_2O)_5]^{2+}$ complex of Cu^{2+} transforms upon reduction to the linear $[Cu(H_2O)_2]^+$ trimer expelling three H_2O molecules from the first coordination shell. For a discussion of this interesting effect we refer to Refs 9 and 12. The focus of the present publication is on more technical issues. Thus comparing the results of the CP2K and CPMD simulations we notice that the results for geometry basically agree. The

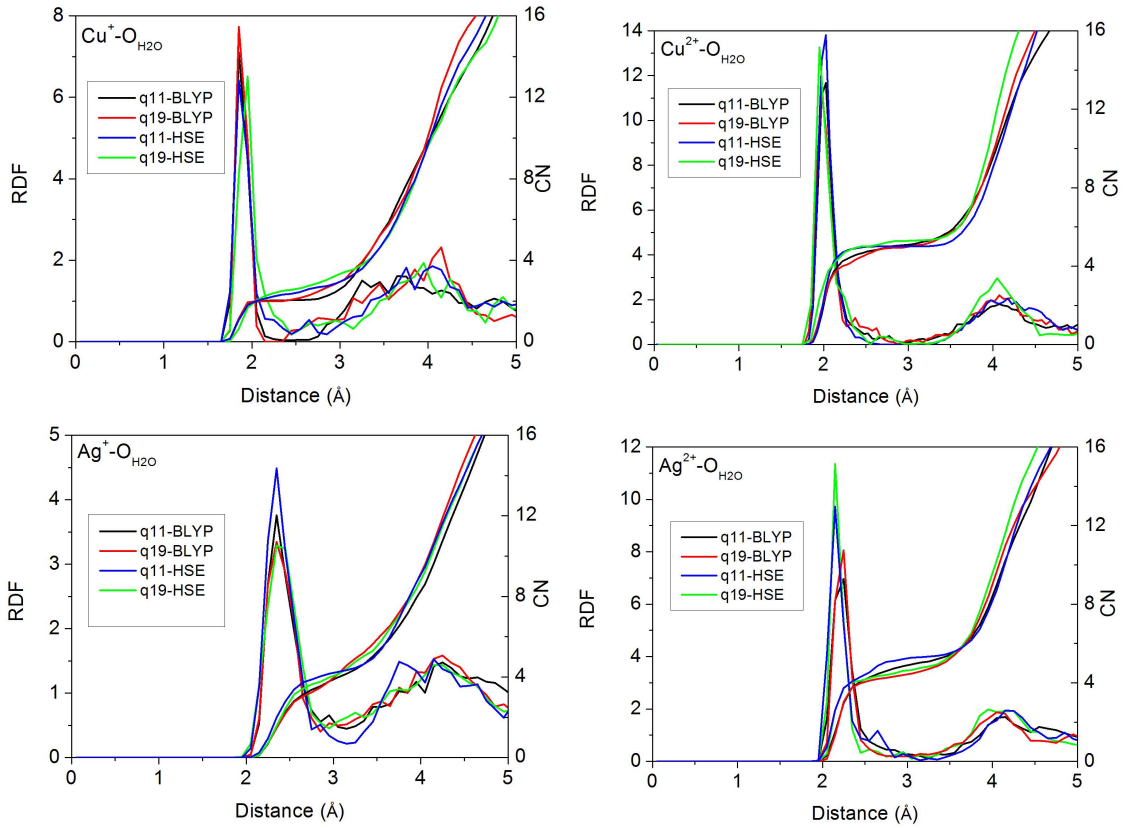

Figure 3: the metal oxygen RDFs (radial distribution functions) and CNs (coordination numbers).

first RDF peaks for Cu^{1+}-O and Cu^{2+}-O in the RDF's of fig. 3 are positioned at $1.85 \sim 1.90$Å and $1.95 \sim 2.01$Å, respectively, which is very close to the corresponding CPMD distances of 1.85Å and 1.99Å for the Cu mono and dication.

A key observation of our first DFTMD study of the redox chemistry of the Cu and Ag aquacations of more than a decade ago[9] was that, while the coordination of the dication is similar (approximately five coordinated) the response to the addition of an electron is less drastic for Ag than it is for Cu. In the case of reduction of Ag^{2+} only one water molecule left the first hydration shell. This could again be confirmed in the present calculation. For Ag^{1+}, all four combinations of functional and pseudopotentials predict the first RDF peaks to be located at 2.35Å. For Ag^{2+}, the first peaks of the two HSE06 RDFs (2.15Å) have moved in by 0.1Å compared to the two BLYP RDFs (2.25Å), consistent with the shorter Ag-O bonds in the gas-phase $[Ag(H_2O)_5]^{2+}$ complexes (table 1). The main conclusion is

again that where the geometry is concerned the BLYP results of Ag^{1+} and Ag^{2+} agree with previous q11-BLYP based CPMD simulation.

Redox potentials

Contrary to the geometry, the redox potentials of the Cu and Ag aqua cations computed using the latest CP2K technology show significant differences with previous CPMD estimates. The results are compared in table 3. The CPMD estimates are taken from two papers by Jochen Blumberger, namely Ref. 12 for Cu and Ref. 11 for Ag. The calculations in Refs 11 and 12 were based on the same free energy perturbation scheme for reversible insertion/removal of electrons as used here (Eq. 5). The resulting thermodynamic integrals, indicated by AIP in the notation of the present paper, are repeated in table 3 and have been converted to potentials on the SHE scale using the MDHE method developed later (Eqs. 9 and 10). This gives $U^\circ = -1.13$V for the Cu^{1+}/Cu^{2+} couple and $U^\circ = 0.35$V for Ag^{1+}/Ag^{2+} as also indicated in the table. While the relative value of U°, i.e the free energy change $e_0\Delta U^\circ = -1.48$ eV of the redox reaction $Cu^{1+} + Ag^{2+} \rightarrow Cu^{2+} + Ag^{1+}$ is in good agreement with experiment ($e_0\Delta U^\circ = -1.66$eV) the absolute values of U° are underestimated by more than 1V.

The obvious suspect to blame for the large discrepancy of the absolute redox potentials is underestimation of IP's by the GGA. A first priority for us was therefore to verify that the CP2K calculations are consistent with the CPMD estimates. They are not. CP2K improves on CPMD by a positive shift of 0.6 to 0.7 eV for both Cu an Ag as can be seen from the data in table 3. Both calculations use the same GGA functional (BLYP) and a 11 electron valence electron pseudopotential (PP) referred to as q11-BLYP in the table. The difference is that the PP used in CPMD (Trouiller-Martins[55]) is significantly softer than the dual space PP's[57,58] used in CP2K. The details of PP's evidently do matter for the ionization of d^{10} ions. Indeed, including the ns^2np^6 core together with the nd^{11} electrons in the valence leads to further improvements. In fact the q19-BLYP estimate for Cu^{1+}/Cu^{2+}

Table 3: Ionization potentials (IP) in units of eV of the Cu^{1+} and Ag^{1+} aqua ions in various approximations. η is the coupling parameter in the thermodynamic integral (Eq. 5) for the estimation of the adiabatic ionization potential under periodic boundary conditions (AIP(pbc)). The AIP(pbc) given in the table is the estimate obtained from a finite set of vertical IP's listed in columns labelled by the η values for which they were computed. U° is the corresponding redox potentials vs SHE obtained using the computational hydrogen electrode (Eqs. 9 and 10).

		$\eta = 0.0$	$\eta = 0.25$	$\eta = 0.5$	$\eta = 0.75$	$\eta = 1.0$	AIP(pbc)	U°
		Cu^{1+}/Cu^{2+} (Exp.=0.16)						
CP2K	q11-BLYP	2.20	1.31	0.08	−0.56	−1.14	0.35	−0.46
	q11-HSE	2.10		−0.59		−2.00	−0.29	−1.10
	q19-BLYP	2.23	1.89	0.39	0.02	−0.79	0.82	0.01
	q19-HSE	2.78	1.54	0.51	−0.37	−1.20	0.61	−0.20
CPMD[12]	q11-BLYP	2	0.57	−0.75	−1.25	−1.75	−0.32	−1.13
		Ag^{1+}/Ag^{2+} (Exp.=1.98)						
CP2K	q11-BLYP	2.45		2.06		0.45	1.91	1.10
	q11-HSE	3.35		1.72		0.01	1.71	0.90
	q19-BLYP	2.48		2.20		0.49	1.96	1.15
	q19-HSE	3.83	3.20	2.65	1.49	0.76	2.53	1.72
CPMD[11]	q11-BLYP	2.03	1.87	1.17	0.61	−0.05	1.16	0.35

is in good agreement with experiment being about 0.2V too small. The q19-BLYP value for Ag^{1+}/Ag^{2+} is, however, still rather far off (0.8V too small). The 0.8V error in the CP2K-q19-BLYP potential for Ag^{1+}/Ag^{2+}, while large, however still compares favourably with the huge error of 1.6V in the CPMD-q11-BLYP calculation.

Including exact exchange, of course, does have an effect, but it is not necessarily positive. The Cu^{1+}/Cu^{2+} couple is a good example. Changing over from BLYP to HSE06 makes the redox potential again too cathodic. The negative change in U° for the q11 PP is particularly drastic, −0.64V. However also for q19 there still is a (minor) decrease of −0.2V. For Ag^{1+}/Ag^{2+}, on the other hand, mixing in exact exchange helps. While the q11-HSE06 potential is still marginally lower compared to q11-BLYP, the q19-HSE06 combination increases U° to 1.72V, less than 0.3V short of the experimental value of 1.98V.

How can we understand the variation of the redox potential with computational method? The improvement of q19 over q11 PP's is perhaps not unexpected. It confirms that ionization of a closed shell nd^{10} ion polarizes the ns^2np^6 shell below it. This is also supported by the gas-phase IP calculations (table 2). The disappointing performance of HSE06 for Cu is probably related to the observation made in quantum chemistry that the fraction of exact exchange suitable for main group chemistry ($\sim 25\%$) is too high for first row transition metal complexes.[72,73] However, can these effects, familiar from the literature on gas-phase transition metal cluster calculations, also explain the pronounced difference in behaviour between the Cu and Ag aqua cations? Why is HSE06 working so well for Ag compared to the GGA while it does worse for Cu?

With a reduction potential vs SHE of 0.16V, Cu^{2+} can be considered a redox neutral cation or a very mild oxidant. The reduction potential of Ag^{2+} is 1.98V, making it a most aggressive oxidant. In fact, U° for Ag^{2+}/Ag^{1+} is comparable to that of the $OH^\bullet/OH^-$ couple (1.9V vs SHE). As discussed in the introduction, the oxidation of the hydroxide anion was our model system of choice for the validation of the DFTMD methodology for redox potential calculation.[17,28] The vertical IP of OH^- is close enough to the valence band of the solvent to lead to hybridization of the HOMO of the solute and the water VBM. In Ref. 17 we argued that this effect, which is not an artefact of the DFT but physical,[23] can lead to underestimation of the adiabatic ionization potential if the IP of the aqueous solvent is underestimated by as much as it is in the GGA (more than 3eV, see below). We believe that the same analysis applies to Ag^{2+} and that this can also explain the difference with Cu^{2+}.

Energy level diagram

The argument in Ref. 17 is an application of Marcus theory to ionization half reactions (see also Refs. 31,32). The essence of the theory can be summarized in a level diagram combining the vertical detachment level ($-$IP) of the reduced form of a species and the vertical attachment level ($-$EA) of the oxidized form with the redox level $-e_0U$ ("Marcus

triplet"). Figure 4 shows such a diagram for the q19 data of table 3. The IP levels have been obtained from the vertical ionization gaps at $\eta = 0$ in table 3 according to Eq. 11. Similarly the EA levels are the vertical gaps at $\eta = 1$ relative to the SHE reference (see Eq. 12).

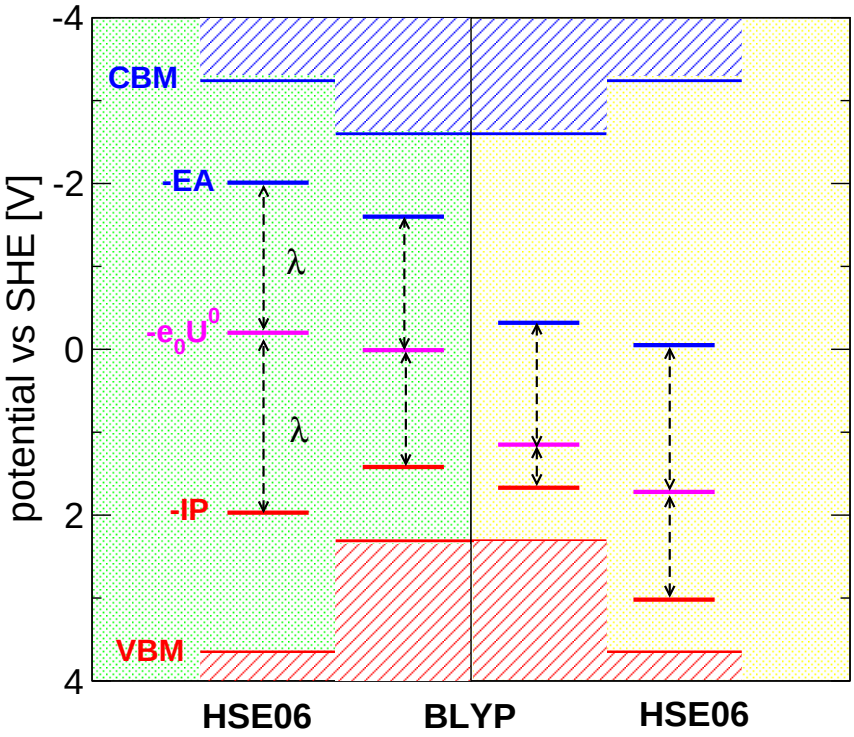

Figure 4: Computed energy levels of the Cu^{1+}/Cu^{2+} (green panel) and Ag^{1+}/Ag^{2+} (yellow panel) aqua-cations compared to the valence band maximum (VBM) and conduction band minimum (CBM) of liquid water. Only the q19 energies of table 3 are represented. The vertical ionization potential (IP) of a monocation is indicated in red, the vertical electron affinity (EA) of a dication in blue, the redox potential (e_0U°) in magenta with the corresponding colour convention for the band edges of water. λ is the reorganization energy. All levels have been aligned wrt to the SHE using the molecular dynamics hydrogen electrode. The water energies are the same as in Ref. 17.

In DFTMD simulation the electronic states of the solute are allowed to interact with the extended states of the solvent and the relative position of the solvent bandedges is therefore important information quantifying the strength of this interaction. The energies of the one-electron states of liquid water can be aligned with the SHE using the same molecular dynamics hydrogen electrode method.[17,38] On this electrochemical scale the experimental VBM and CBM are at 5.5V and −3.2 V (not shown). A discussion of the experimental data

and relevant references to the literature can be found in Ref. 38 which is also the source for the computational estimates. BLYP badly misaligns the VBM at 2.31V vs SHE, placing the VBM more than 3 eV above the experimental band edge. The CBM corresponds according to BLYP to a negative potential of −2.60V vs SHE. While below the experimental CBM the discrepancy of 0.6 V is not as serious as for the VBM. HSE06 gives better estimates with the VBM at 3.65V and the CBM at −3.24V vs SHE. The CBM (minus the EA) is basically in the right place but the IP of liquid water is still underestimated by 1.85 V in the HSE06 approximation.

Focusing first on the BLYP levels in fig. 4 we note that, in spite of the large difference in redox potential between Ag^{1+} and Cu^{1+} (1.8 V according to experiment) the −IP levels are virtually aligned (the difference in energy is only 0.25 eV). Another suspicious feature is the pronounced asymmetry in the reorganization energies for the Ag^{1+}/Ag^{2+} couple. The gap between the −IP level and the redox level is a factor three smaller than the gap between −EA and $-e_0U$. The Cu^{1+}/Cu^{2+} triplet is more symmetric which is the normal linear response (Marcus) behaviour. However, the proximity of the −IP level to the VBM of water in the BLYP approximation suggests that the Ag^{1+} and Cu^{1+} vertical IP levels are effectively pinned by the water valence band. Indeed, switching to HSE06, the detachment level of Ag^{1+} follows the VBM down. The Cu^{1+} level does too, but only by a relatively small amount suggesting that the coupling to the H_2O valence band states has weakened. In comparison, the vertical attachment levels (−EA) of the dications are less sensitive to the details of the functional, consistent with what was observed in Ref. 17 for the set of small (neutral) radicals we studied there.

For Ag^{2+}/Ag^{1+} HSE06 effectively restores the reorganization energy symmetry as required by linear response approximation of Marcus theory. The non-linearity in the GGA for this couple is a spurious electronic effect due to hybrization with the extended states of the solvent as we observed for $OH^{\bullet}/OH^{-}$.[17] This shows that the energy position of the VBM of the solvent plays a crucial role in our interpretation of the effect of exact exchange

on redox potentials. The GGA places the VBM way too high pushing up the detachment levels of solutes. The more oxidative, the more sensitive are the solutes to interaction with the misaligned VBM. This is the main explanation of the large increase in redox potential as calculated for the Ag^{1+}/Ag^{2+} reaction by HSE06 compared to BLYP.

Finite system size effects

The theory underlying the DFTMD calculation has been formulated for infinite dilution as required by the definition of standard states in solution chemistry. These conditions are approximated by periodic model systems containing a single ion and a homogeneous distribution of counter charge. Provided the body of solvent is sufficiently large, the interaction between periodic images of the ion and the neutralizing background can be ignored. The bias in the electrostatic reference, V_0, remains finite. However, for vanishing concentration of solutes, V_0 is determined by the solvent and therefore cancels in the reduction potential *vs* SHE. This is the idea behind the half reaction implementation of the molecular dynamics hydrogen electrode. The half reaction scheme has been validated in Ref. 51 by comparing the acidity of a number of small acids to experiment. pK_a calculations are preferred for this purpose because acid dissociation is closed shell chemistry for which the DFT approximation is less critical.

Our DFTMD model systems are rather small. The supercell has a length of ≈ 10Å(see method section). The system has a net charge and finite size effects can be significant. However, because of the exceptionally high dielectric constant of water ($\epsilon \approx 80$) screening is very effective. Finite system size errors, while not negligible, are in fact not the dominant source of error in DFTMD redox potential calculations. Screening in polar liquids is traditionally taken into account by the Born cavity model or extensions thereof. Hummer and colleagues have extended this model to systems under periodic boundary conditions.[74–78] The result is an expression in powers of $1/L$ where L is the size of the cubic periodic cell.

The leading $1/L$ term in the finite size error is multiplied by $1/\epsilon$ and effectively vanishes

for aqueous ions. The next term is equal to $2\pi q^2 R^2/(3e_0 L^3)$ where R is the cavity radius and q the charge of the ion (see also earlier work by Felderhof[79]). This term is zero order in $1/\epsilon$ and determines in practice the finite size error in solvation free energy of classical point charge models of aqueous ions.[78] The correction to the U° of the $OH^\bullet/OH^-$ reaction is less than 100mV, which is within the statistical uncertainty (100 to 200mV) of the DFTMD calculations.

Finite size effects for aqua cations can be expected to be significantly larger. The error for the oxidation of a M^{q+} cation is proportional to $(q+1)^2-q^2$ and also scales with the square of the Born radius R. Fitting R to the experimental solvation free energy gives for Cu^{1+}/Cu^{2+} a correction of $\Delta U^\circ = 0.6$V. For Ag^{1+}/Ag^{2+} we find $\Delta U^\circ = 0.9$V. These corrections must be added to the potentials in table 3. Taking the q19-HSE06 results as our best estimate, this would lead to an *overestimate* of 0.2V for the redox potential of Cu^{1+}/Cu^{2+} and as much as 0.6V for Ag^{1+}/Ag^{2+}. However, these corrections based on a classical point charge model are almost certainly an exaggeration. We are currently investigating this question in a detailed DFTMD study of the Fe^{2+}/Fe^{3+} aqua ion oxidation. Preliminary results indicate that the finite size correction is at least half the size of the classical point charge prediction. If true, this would bring the results of table 3 within 0.3V of the experimental value.

The parallel between redox active ions in solution and charged defects in a semiconductor played an important role in the interpretation of our results. We made this comparison to support the claim that electronic interactions between the localized states of the impurity and the extended states of the environment can be an issue in DFTMD simulation. In this context, we should point out that corrections for finite size effects of periodic supercells containing charged point defects have a long tradition in computational solid state physics.[42,80–86] Some of the more recent treatments are rather sophisticated and seem to perform well.[42,84–86] This raises the question whether these schemes could be applied to redox potential calculations in aqueous systems. This is not as straightforward as it may seem at first. The dielectric response in water is almost entirely ionic (inertial). Moreover, the

ionic screening is so powerful that water behaves effectively as a metal ($1/\epsilon \approx 0$). This may require some modification of the solid state correction schemes. This is another issue currently under investigation.

Discussion and outlook

In this technical contribution we have revisited the problem of the computation of the standard potentials of the aqueous Cu^{1+}/Cu^{2+} and Ag^{1+}/Ag^{2+} redox couples using all-atom DFTMD methods. Both reactions involve the removal of an electron from a filled d^{10} shell. We encountered a number of technical problems, such as polarization of the *sp* shell with the same principle quantum number as the *d* electrons and the sometimes ambivalent effect of exact exchange. These issues are familiar from quantum chemistry calculations of coordination complexes in vacuum or embedded in an implicit solvent.

In addition, because of the large difference in redox potential (1.8V), the Cu^{1+}/Cu^{2+} and Ag^{1+}/Ag^{2+} redox couples are also good models to investigate a typical electronic condensed phase effect, namely the hybridization with the extended states of the valence band of the solvent. The ionization of Ag^{1+} is much more sensitive to this effect than the ionization of Cu^{1+}.The reason is that the levels of Cu^{1+}/Cu^{2+} are midgap states while the levels of Ag^{1+}/Ag^{2+} are closer the valence band maximum of the solvent. This also explains why mixing in exact exchange has a significant effect on the DFT estimate of the redox potential of Ag^{1+}/Ag^{2+} while the effect is only minor for Cu^{1+}/Cu^{2+}. The effect is partly due to the increase of the ionization potential of the solvent and is therefore indirect.

DFTMD calculation of redox potentials is orders of magnitude more expensive than implicit solvent or QM/MM based calculations. This is because interaction with the extended states of the solvent is ignored in these schemes. Allowing for such interactions not only increases the computational costs but also exposes us to all the nasty effects of the delocalization or band gap error familiar form the DFT study of charged defects in semiconductors.

It takes additional effort to overcome these errors, which was the subject of this paper. The experience of the computational solid state community has been of definite help in identifying and understanding the confusing errors in the DFTMD calculations. The work on charged defects in solids has also shown that the results of standard hybrid functions can be further improved by optimizing the fraction of exact exchange.[44,87] Alternatively the application of many body perturbation methods in the G0W0 approximation has been explored. Particularly relevant in the present context are G0W0 calculations of charge transition levels of defects in ionic solids with a bandgap similar to water such as SiO_2, MgO and LiF.[45,48,49] Galli and coworkers have developed an implementation of the G0W0 method suitable for the application to aqueous systems.[67] The first studies using this method confirm that adding a G0W0 derived correction to DFT orbital energies leads to more accurate estimates of ionization energies of solutes[30,88] and the pure liquid.[89] Finally we mention the development of MP2, RPA methods for condensed phase systems[90] which already have been applied to liquid water[91] but not yet to aqueous solutes.

We have identified hybridization of localized solute states with the extended of the solvent as an major source of error in calculations of vertical and adiabatic ionization energies. However, for shallow defects or resonant impurity states in semiconductors the interaction with band states is a real effect. As recent PES experiments by the Winter group show, a such situation may also occur in aqueous redox chemistry. An interesting example is the PES signal of aqueous Fe^{3+} which is merged with the valence band of water.[5] The ionization product, the Fe^{4+} (ferryl) ion, is a potent redox catalyst. We conclude this paper, therefore, with the still somewhat speculative statement, that extended states of the solvent have a role to play in redox catalysis by strong oxidants such as Fe^{4+} or also $OH^{\bullet}$ and $Cl^{\bullet}$ and should therefore be taken into account in computational studies.

Acknowledgement

We thank Mathias Krack for supplying us with the 19 valence electron pseudo potentials for Cu and Ag and Florian Schiffman for the corresponding q19 basis sets. We acknowledge grants from the National Science Foundation of China (Nos. 41002013, 41222015 and 41273074) and Newton International Fellowship program. Further support came from the State Key Laboratory for Mineral Deposits Research in Nanjing University and the Foundation for the Author of National Excellent Doctoral Dissertation of PR China (No.201228). We are grateful to the High Performance Computing Center of Nanjing University for allowing us to use the IBM Blade cluster system.

References

(1) Wang, L.-P.; Van Voorhis, T. A Polarizable QM/MM Explicit Solvent Model for Computational Electrochemistry in Water. *J. Chem. Theor. Comp.* **2012**, *8*, 610–617.

(2) Li, J.; Fisher, L.; Chen, J. L.; Bashford, D.; Noodleman, L. Calculation of Redox Potentials and pKa Values of Hydrated Transition Metal Cations by a Combined Density Functional and Continuum Dielectric Theory. *Inorg. Chem.* **1996**, *35*, 4694.

(3) Uudsemaa, M.; Tamm, T. Density-Functional Theory Calculations of Aqueous Redox Potentials of Fourth-Period Transition metals. *J. Phys. Chem. A* **2003**, *107*, 9997–10003.

(4) Jaque, P.; V., M. A.; Cramer, C. J.; Truhlar, D. Computational Electrochemistry: The Aqueous $Ru^{3+}|Ru^{2+}$ Reduction Potential. *J. Phys. Chem. C* **2007**, *111*, 5783–5799.

(5) Seidel, R.; Thürmer, S.; Moens, J.; Geerlings, P.; Blumberger, J.; Winter, B. Valence Photoemission Spectra of Aqueous $Fe^{2+/3+}$ and $[Fe(CN)_6]^{4-/3-}$ and their Interpretation by DFT Calculations. *J. Phys. Chem. B* **2011**, *115*, 11671–11677.

(6) Marenich, A. V.; Majumdar, A.; Lenz, M.; Cramer, C. J.; Truhlar, D. G. Construction of Pourbaix Diagrams for Ruthenium-Based Water-Oxidation Catalysts by Density Functional Theory. *Angew. Chem., Int. Ed. Engl.* **2012**, *51*, 12810 V12814.

(7) Marenich, A. V.; Ho, J.; Coote, M. L.; Cramer, C. J.; Truhlar, D. G. Computational Electrochemistry: Prediction of Liquid-Phase Reduction Potentials. *Phys. Chem. Chem. Phys* **2014**, *asap*, DOI: 10.1039/c4cp01572j.

(8) Zeng, X.; Hu, H.; Hu, X.; Cohen, A. J.; Yang, W. Ab Initio Quantum Mechanical/Molecular Mechanical Simulation of Electron Transfer Process: Fractional Electron Approach. *J. Chem. Phys.* **2008**, *128*, 124510.

(9) Blumberger, J.; Bernasconi, L.; Tavernelli, I.; Vuilleumier, R.; Sprik, M. Electronic Structure and Solvation of Copper and Silver Ions: A Theoretical Picture of a Model Aqueous Redox Reaction. *J. Am. Chem. Soc.* **2004**, *126*, 3928–3938.

(10) Tateyama, Y.; Blumberger, J.; Sprik, M.; Tavernelli, I. Density Functional Molecular Dynamics Study of the Redox Reactions of Two Anionic Aqueous Transition Metal Complexes. *J. Chem. Phys.* **2005**, *122*, 234505.

(11) Blumberger, J.; Tavernelli, I.; Klein, M. L.; Sprik, M. Diabatic Free Energy Curves and Coordination Fluctuations for the Aqueous Ag^{+}/Ag^{2+} Redox Couple: A Biased Born-Oppenheimer Molecular Dynamics Investigation. *J. Chem. Phys.* **2006**, *124*, 064507.

(12) Blumberger, J. Cu^{+}_{aq}/Cu^{2+}_{aq} Redox Reaction Exhibits Strong Nonlinear Solvent Response Due to Change in Coordination Number. *J. Am. Chem. Soc.* **2008**, *130*, 16065.

(13) Seidel, R.; Faubel, M.; Winter, B.; Blumberger, J. Single-ion Reorganization Free Energy of Aqueous $Ru(bpy)_3^{2+/3+}$ and $Ru(H_2O)_6^{2+/3+}$ from Photoemission Spectroscopy and Density Functional Molecular Dynamics Simulation. *J. Am. Chem. Soc.* **2009**, *131*, 16127–16137.

(14) Moens, J.; Seidel, R.; Geerlings, P.; Faubel, M.; Winter, B.; Blumberger, J. Energy Levels and Redox Properties of Aqueous $Mn^{2+/3+}$ from Photoemission Spectroscopy and Density Functional Molecular Dynamics Simulation. *J. Phys. Chem. B* **2010**, *114*, 9173–9182.

(15) Car, R.; Parrinello, M. Unified Approach for Molecular Dynamics and Density-Functional Theory. *Phys. Rev. Lett.* **1985**, *55*, 2471–2474.

(16) Marx, D.; Hutter, J. *Ab Initio Molecular Dynamics: Basic Theory and Advanced Methods*; Cambridge University Press: Cambridge, 2009.

(17) Adriaanse, C.; Cheng, J.; Chau, V.; Sulpizi, M.; VandeVondele, J.; Sprik, M. Aqueous Redox Chemistry and the Electronic Band Structure of Liquid Water. *J. Phys. Chem. Lett.* **2012**, *3*, 3411–3415.

(18) Stanbury, D. M. Reduction Potentials Involving Inorganic Free Radicals in Aqueous Solution. *Adv. Inorg. Chem.* **1989**, *33*, 69–138.

(19) Becke, A. D. Density-Functional Exchange-Energy Approximation with Correct Asymptotic Behaviour. *Phys. Rev. A* **1988**, *38*, 3098–3100.

(20) Lee, C.; Yang, W.; Parr, R. Development of the Colle-Salvetti Correlation-Energy Formula into a Functional of Electron-Density. *Phys. Rev. B* **1988**, *37*, 785–789.

(21) Winter, B.; Faubel, M. Photoemission from Liquid Aqueous Solutions. *Chem. Rev.* **2006**, *106*, 1176–1211.

(22) Seidel, R.; Thürmer, S.; Winter, B. Photoelectron Spectroscopy Meets Aqueous Solutions: Studies from a Vacuum Liquid Microjet. *J. Phys. Chem. Lett.* **2011**, *2*, 633–641.

(23) Winter, B.; Faubel, M.; Hertel, I. V.; Pettenkofer, C.; Bradforth, S. E.; Jagoda-Cwiklik, B.; Cwiklik, L.; Jungwirth, P. Electron Binding Energies of Hydrated H_3O^+

and OH^-: Photoelectron Spectroscopy of Aqueous Acid and Base Solutions Combined with Electronic Structure Calculations. *J. Am. Chem. Soc.* **2006**, *128*, 3864–3865.

(24) Pluharova, E.; Oncak, M.; Seidel, R.; Schroeder, C.; Schroeder, W.; Winter, B.; Bradforth, S. E.; Jungwirth, P.; Slavicek, P. Transforming Anion Instability into Stability: Contrasting Photoionization of Three Protonation Forms of the Phosphate Ion upon Moving into Water. *J. Phys. Chem. B* **2012**, *116*, 13254–13264.

(25) Jagoda-Cwiklik, B.; Slavicek, P.; Cwiklik, L.; Nolting, D.; Winter, B.; Jungwirth, P. Ionization of Imidazole in the Gas Phase, Microhydrated Environments, and in Aqueous Solution. *J. Phys. Chem. A* **2008**, *112*, 3499–3505.

(26) Gosh, D.; Roy, A.; Seidel, R.; Winter, B.; Bradforth, S. E.; Krylov, A. I. First-Principle Protocol for Calculating Ionization Energies and Redox Potentials of Solvated Molecules and Ions: Theory and Application to Aqueous Phenol and Phenolate. *J. Phys. Chem. B* **2012**, *116*, 7269–7280.

(27) Thürmer, S.; Seidel, R.; Winter, B. Flexible H_2O_2 in Water: Electronic Structure from Photoelectron Spectroscopy and Ab Initio Calculations. *J. Phys. Chem. A* **2011**, *115*, 6239–6249.

(28) Adriaanse, C.; Sulpizi, M.; VandeVondele, J.; Sprik, M. The Electron Attachment Energy of the Aqueous Hydroxyl Radical Predicted from the Detachment Energy of the Aqueous Hydroxide Anion. *J. Am. Chem. Soc.* **2009**, *131*, 6046–6047.

(29) Opalka, D.; Sprik, M. Solute-Solvent Charge-Transfer Excitations and Optical Absorption of Hydrated Hydroxide from Time-Dependent Density-Functional Theory. *J. Chem. Theor. Comp.* **2014**, *10*, 2465–2470.

(30) Opalka, D.; Pham, T.; Sprik, M.; Galli, G. The Ionization Potential of Aqueous Hydroxide Computed Using Many-Body Perturbation Theory. *J. Chem. Phys.* **2014**, *141*, 034501.

(31) Von Burg, K.; Delahay, P. Photo Emission Spectroscopy of Inorganic Anions in Aqueous Solution. *Chem. Phys. Lett.* **1981**, *78*, 287–290.

(32) Delahay, P. Photoelectron Emission Spectroscopy of Aqueous Solutions. *Acc. Chem. Res.* **1982**, *15*, 40–45.

(33) Aziz, E. F.; Ottoson, N.; Faubel, M.; Hertel, I. V.; Winter, B. Interaction between Liquid Water and Hydroxide revealed by Core-Hole De-Excitation. *Nature* **2008**, *455*, 89–91.

(34) Trasatti, S. The Absolute Electrode Potential: An Explanatory Note. *Pure & Appl. Chem.* **1986**, *58*, 955–966.

(35) Fawcett, W. R. The Ionic Workfunction and its Role in Estimating Absolute Electrode Potentials. *Langmuir* **2008**, *24*, 9868–9875.

(36) Winter, B.; Weber, R.; Widdra, W.; Dittmar, M.; Faubel, M.; Hertel, I. V. Full Valence Band Photoemission from Liquid Water Using EUV Synchrotron Radiation. *J. Phys. Chem. A* **2004**, *108*, 2625.

(37) Cheng, J.; Sulpizi, M.; VandeVondele, J.; Sprik, M. Hole Localization and Thermochemistry of Oxidative Dehydrogenation of Aqueous Rutile TiO_2(110). *ChemCatChem* **2012**, *4*, 636–640.

(38) Cheng, J.; Sprik, M. Alignment of Electronic Energy Levels at Electrochemical Interfaces. *Phys. Chem. Chem. Phys* **2012**, *14*, 11245–11267.

(39) Zhang, C.; Pham, T. A.; Gygi, F.; Galli, G. Electronic Structure of the Solvated Chloride Anion from First Principles Molecular Dynamics. *J. Chem. Phys.* **2013**, *138*, 181102.

(40) Ge, L.; Bernasconi, L.; Hunt, P. Linking Electronic and Molecular Structure: Insight into Aqueous Chloride Solvation. *Phys. Chem. Chem. Phys* **2013**, *15*, 13169–13183.

(41) VandeWalle, C. G.; Janotti, A. Advances in Electronic Structure Methods for Defects and Impurities in Solids. *Phys. Status Solidi B* **2011**, *248*, 19–27.

(42) Freysoldt, C.; Grabowski, B.; Hickel, T.; Neugebauer, J.; Kresse, G.; Janoti, A.; VandeWalle, C. G. First-Principles Calculations of Point Defects in Solids. *Rev. Mod. Phys.* **2014**, *86*, 253–305.

(43) Deak, P.; Gali, A.; Aradi, B.; Frauenheim, T. Accurate Gap Levels and their Role in the Reliability of Other Calculated Defect properties. *Phys. Status Solidi B* **2011**, *248*, 790–798.

(44) Alkauskas, A.; Broqvist, P.; Pasquarello, A. Defect Levels through Hybrid Density Functionals: Insights and Applications. *Phys. Status Solidi B* **2011**, *248*, 775–789.

(45) Chen, W.; Pasquarello, A. Correspondence of Defect Energy Levels in Hybrid Density Functional Theory and Many-Body Perturbation Theory. *Phys. Rev. B* **2013**, *88*, 115104.

(46) Raebiger, H.; Lany, S.; Zunger, A. Charge Self-Regulation on Changing the Oxidation State of Transition Metals in Insulators. *Nature* **2008**, *453*, 763–766.

(47) Rinke, P.; Janottti, A.; Scheffler, M.; Van de Walle, C. G. Defect Formation Energies without the Band-Gap Problem: Combining Density-Functional Theory and the GW Approach for the Silicon Self-Interstitial. *Phys. Rev. Lett.* **2009**, *102*, 026402.

(48) Martin-Samos, L.; Roma, G.; Rinke, P.; Y., L. Charged Oxygen Defects in SiO_2: Going beyond Local and Semilocal Approximations to Density Functional Theory. *Phys. Rev. Lett.* **2010**, *104*, 075502.

(49) Rinke, P.; Schleife, A.; Kioupakis, E.; Janotti, A.; Roödl, C.; Bechstedt, F.; Scheffler, M.; Van de Walle, C. G. First-Principles Optical Spectra for F Centers in MgO. *Phys. Rev. Lett.* **2012**, *108*, 126404.

(50) Cheng, J.; Sulpizi, M.; Sprik, M. Redox Potentials and pKa for Benzoquinone from Density Functional Theory Based Molecular Dynamics. *J. Chem. Phys.* **2009**, *131*, 154504.

(51) Costanzo, F.; Della Valle, R. G.; Sulpizi, M.; Sprik, M. The Oxidation of Tyrosine and Tryptophan Studied by a Molecular Dynamics Normal Hydrogen Electrode. *J. Chem. Phys.* **2011**, *134*, 244508.

(52) Sulpizi, M.; Sprik, M. Acidity Constants from Vertical Energy Gaps: Density Functional Theory Based Molecular Dynamics Implementation. *Phys. Chem. Chem. Phys* **2008**, *10*, 5238–5249.

(53) Guidon, M.; Hutter, J.; VandeVondele, J. Auxiliary Density Matrix Methods for Hartree-Fock Exchange Correlations. *J. Chem. Theor. Comp.* **2010**, *6*, 2348–2364.

(54) CPMD Version 3.8.2, The CPMD consortium, `http://www.cpmd.org`, MPI für Festkörperforschung and the IBM Zurich Research Laboratory, 2004.

(55) Troullier, N.; Martins, J. Efficient Pseudopotentials for Plane-Wave Calculations. *Phys. Rev. B* **1991**, *43*, 1993.

(56) The CP2K developers group, `http://www.cp2k.org`, 2008.

(57) Goedecker, S.; Teter, M.; Hutter, J. Separable Dual-Space Gaussian Pseudopotentials. *Phys. Rev. B* **1996**, *54*, 1703.

(58) Hartwigsen, C.; Goedecker, S.; Hutter, J. Relativistic Separable Dual-Space Gaussian Pseudopotenials from H to Rn. *Phys. Rev. B* **1998**, *58*, 3641.

(59) Lyde, D. R., Ed. *CRC Handbook of Chemistry and Physics*, 84th ed.; CRC Press: Boca Raton, 2003.

(60) Tavernelli, I.; Vuilleumier, R.; Sprik, M. Ab Initio Molecular Dynamics for Molecules with Variable Numbers of Electrons. *Phys. Rev. Lett.* **2002**, *88*, 213002.

(61) Cascella, M.; Magistrato, A.; Tavernelli, I.; Carloni, P.; Rothlisberger, U. Role of Protein Frame and Solvent for the Redox Properties of Azurin from Pseudomonas Aeruginosa. *Proc. Natl. Acad. Sci. USA* **2006**, *103*, 19641V19646.

(62) Krukau, A. V.; Vydrov, O. A.; Izmaylov, A. F.; Scuseria, G. E. Influence of the Exchange Screening Parameter on the Performance of Screened Hybrid Functionals. *J. Chem. Phys.* **2006**, *125*, 224106.

(63) King, G.; Warshel, A. Investigation of the Free Energy Functions for Electron Transfer Reactions. *J. Chem. Phys.* **1990**, *93*, 8682–8692.

(64) Hunt, P.; Sprik, M. On the Position of the Highest Molecular Orbital in Aqueous Solutions of Simple Ions. *Comp. Phys. Comm.* **2005**, *6*, 1805.

(65) Leung, K. Surface Potential at the Air-Water Interface Computed Using Density Functional Theory. *J. Phys. Chem. Lett.* **2010**, *1*, 496–499.

(66) Kathmann, S. M.; Kuo, J.; Mundy, C. J.; Schenter, G. K. Understanding the Surface Potential of Water. *J. Phys. Chem. B* **2011**, *115*, 4369–4377.

(67) Pham, T. A.; Nguyen, H.-V.; Rocca, D.; Galli, G. GW Calculations Using the Spectral Decomposition of the Dielectric Matrix: Verification, Validation, and Comparison of Methods. *Phys. Rev. B* **2013**, *87*, 155148.

(68) Isse, A. A.; Gennaro, A. Absolute Potential of the Standard Hydrogen Electrode and the Problem of Interconversion of Potentials in Different Solvents. *J. Phys. Chem. B* **2010**, *114*, 7894–7899.

(69) Hutter, J.; Iannuzzi, M.; Schiffmann, F.; VandeVondele, J. CP2K : Atomistic Simulations of Condensed Matter Systems. *WIREs Comput. Mol. Sci.* **2014**, *4*, 15–25.

(70) VandeVondele, J.; Krack, M.; Mohamed, F.; Parrinello, M.; Chassaing, T.; Hutter, J.

Quickstep: Fast and Accurate Density Functional Calculations Using a Mixed Gaussian and Plane Waves Approach. *Comp. Phys. Comm.* **2005**, *167*, 103–128.

(71) Martyna, G. J.; Tuckerman, M. E. A Reciprocal Space Based Method for Treating Long Range Interactions in Ab Initio and Force-Field-Based Calculations in Clusters. *J. Chem. Phys.* **1999**, *110*, 2810–2821.

(72) Reiher, M.; O., S.; Hess, B. A. Reparameterization of Hybrid Functionals Based on Energy Differences of States of Different Multiplicity. *Theor. Chem. Acc.* **2001**, *107*, 48–55.

(73) Harvey, J. N. On the Accuracy of Density Functional Theory in Transition Metal chemistry. *Annu. Rep. Prog. Chem., Sect. C* **2006**, *102*, 203–226.

(74) Hummer, G.; Pratt, R. L.; Garcia, A. E. Free Energy of Ion Hydration. *J. Phys. Chem.* **1996**, *100*, 1206–1215.

(75) Hummer, G.; Pratt, L. R.; Garcia, A. E. Ion Sizes and Finite-Size Corrections for Ionic-Solvation Free Energies. *J. Chem. Phys.* **1997**, *107*, 9275–9277.

(76) Hummer, G.; Pratt, L. R.; Garcia, A. E. Molecular Theories and Simulation of Ions and Polar Molecules in Water. *J. Phys. Chem. A* **1998**, *102*, 7885–7895.

(77) Hünenberger, P. H.; McCammon, J. A. Ewald Artifacts in Computer Simulations of Ionic Solvation and Ion-Ion Interaction: A Continuum Electrostatics Theory. *J. Chem. Phys.* **1999**, *110*, 1856–1872.

(78) Ayala, R.; Sprik, M. A Classical Point Charge Model Study of System Size Dependence of Oxidation and Reorganization Free Energies in Aqueous Solution. *J. Phys. Chem. B* **2008**, *112*, 257–269.

(79) Cichocki, B.; Felderhof, B. U.; Hinsen, K. Electrostatic Interactions in Periodic Coulomb and Dipolar Systems. *Phys. Rev. A* **1989**, *39*, 5350.

(80) Leslie, M.; Gillan, M. J. The Energy and Elastic Dipole Tensor of Defects in Ionic Crystals Calculated by the Supercell Method. *J. Phys.: Condens. Matter* **1985**, *18*, 973.

(81) Makov, G.; Payne, M. C. Periodic Boundary Conditions in ab Initio Calculations. *Phys. Rev. B* **1995**, *51*, 4014.

(82) Schultz, P. A. Charged Local Defects in Extended Systems. *Phys. Rev. Lett.* **2000**, *84*, 1942.

(83) Lany, S.; Zunger, A. Assessment of Correction Methods for the Bandgap Problem and for Finite Size Effects in Supercell Defect Calculations: Case Studies for ZnO and GaAs. *Phys. Rev. B* **2008**, *78*, 235104.

(84) Freysoldt, C.; Neugebauer, J.; VandeWalle, C. G. Fully ab Initio Finite-Size Corrections for Charged-Defect Supercell Calculations. *Phys. Rev. Lett.* **2009**, *102*, 016402.

(85) Freysoldt, C.; Neugebauer, J.; VandeWalle, C. G. Electrostatic Interactions between Charged Defects in Supercells. *Phys. Status Solidi B* **2011**, *248*, 1067–1076.

(86) Komsa, H.-P.; Rantala, T. T.; Pasquarello, A. Finite-size Supercell Correction Schemes for Charged Defect Calculations. *Phys. Rev. B* **2012**, *86*, 045112.

(87) Jonathan H. Skone, J. H.; Govoni, M.; Galli, G. Self-Consistent Hybrid Functional for Condensed Systems. *Phys. Rev. B* **2014**, *89*, 195112.

(88) Zhang, C.; Pham, T. A.; Gygi, F.; Galli, G. Communication: Electronic structure of the solvated chloride anion from first principles molecular dynamics. *J. Chem. Phys.* **2013**, *138*, 181102.

(89) Pham, T. A.; Zhang, C.; Schwegler, E.; Galli, G. Probing the Electronic Structure of Water with Many-body Perturbation Theory. *Phys. Rev. B* **2014**, *89*, 060202(R).

(90) Del Ben, M.; Hutter, J.; VandeVondele, J. Electron Correlation in the Condensed Phase from a Resolution of Identity Approach Based on the Gaussian and Plane waves Scheme. *J. Chem. Theor. Comp.* **2013**, *9*, 2654–2671.

(91) Del Ben, M.; Sch´onherr, M.; Hutter, J.; VandeVondele, J. Bulk Liquid Water at Ambient Temperature and Pressure from MP2 Theory. *J. Phys. Chem. Lett.* **2013**, *4*, 3753–3759.